Colloid Polym Sci 277:846–855 (1999)

ORIGINAL CONTRIBUTION

F. Sauzedde
A. Elaïssari
C. Pichot

Hydrophilic magnetic polymer latexes. 1. Adsorption of magnetic iron oxide nanoparticles onto various cationic latexes

Received: 28 December 1998
Accepted in revised form: 15 April 1999

F. Sauzedde · A. Elaïssari (✉) · C. Pichot
Ecole Normale Superieure de Lyon
Unité mixte CNRS-bioMérieux
ENS, 46 allée d'Italie
F-69364 Lyon, France
e-mail: hamid.elaissari@ens-bma.cnrs.fr
Tel.: +33-4-7272-8364
Fax: +33-4-7272-8533

Abstract With a view to preparing monosized hydrophilic functional magnetic latex particles based on a two-step strategy using anionic iron oxide and cationic polymer latexes, the adsorption step was systematically investigated for a better control of the subsequent encapsulation step. The iron oxide nanoparticles were first obtained according to the classical precipitation method of ferric and ferrous chloride salt using a concentrated sodium hydroxide solution, whereas the polystyrene (PS), P(S/*N*-isopropylacrylamide (NIPAM)) core–shell and PNIPAM latexes were produced via emulsion and precipitation polymerizations, respectively. The polymer and inorganic colloids were then characterised. The adsorption of iron oxide nanoparticles onto the three types of polymer latexes via electrostatic interaction was studied as a function of iron oxide particle concentration, charge density and the cross-linking density of the hydrophilic layer. The maximum amounts of magnetic nanoparticles adsorbed onto the various latexes were found to increase in the following order: PS < P(S/NIPAM) < P(NIPAM). This significant difference is discussed by taking into account the charge distribution in the hydrogel layer and diffusion phenomena inside the cross-linked hydrophilic shell.

Key words Cationic latexes · Hydrophilic particles · Iron oxide · Adsorption · Electrostatic interactions

Introduction

In the past ten years, numerous reviews have been devoted to the application of magnetic beads [1–9] in the biomedical field. These composite particles can be used for therapeutic or analytical purposes. In the first case, magnetic particle carriers permit either the guiding and release of a drug in a specific site of the body [6, 10] or the extraction of tumour cells from the organism and their curing in vitro [8, 9]. In both cases, toxicity and the secondary effects of a strong chemical in vivo treatment are avoided. Analytical applications often require a separation step. Magnetic particles were found suitable as a solid phases in immunoassays, since after the capture step the target molecules can easily be separated upon applying a magnetic field [7, 11].

Magnetic particles can be prepared according to three main different strategies.

1. First, inorganic and polymer materials are synthesised separately. Then, polymer chains can be grafted or adsorbed onto an inorganic core, generally composed of iron oxide [12, 13]. Otherwise, when mixed with magnetic material [14, 15], polymer chains can eventually be cross-linked [16, 17] to form large and polydisperse polymer beads containing magnetic material.

2. The second procedure consists of preparing iron oxides inside the polymer particles and was pioneered by Ugelstad and coworkers [18, 19] for preparing supermi-

cron-sized particles; these are currently and successfully used in biomedical applications. Iron salts are directly precipitated inside monodisperse, porous polystyrene (PS) particles. Superparamagnetic iron oxides are formed upon increasing pH and temperature [20, 21]. Magnetic polyacrylamide-based particles have been obtained using a similar method by Kawaguchi et al. [22]. Alternatively, the coating of a poly(S-divinylbenzene-4-vinylpyridine) core by cobalt was achieved by thermolysis of a cobalt salt, allowing magnetic polymer beads to be obtained but with an uneven structure [23].

3. In the third procedure, the polymer is formed onto inorganic particles using heterogeneous batch polymerisation [23–25]. Before polymerisation onto inorganic particles, a surface treatment is performed to increase the affinity between the inorganic particles and the polymer. For example, TiO_2 [26] or Fe_3O_4 [27–29] particles can be coated with a surfactant or can be chemically modified by grafting hydrophobic compounds [30] before performing emulsion polymerisation of S.

Finally, it is worth mentioning the method of Furuzawa et al. [29], which consists of carrying out emulsion polymerisation of S in the presence of polymer seed particles coated with inorganic magnetic nanoparticles. The type of initiator and the amount of surfactant were found to be two important features to avoid coagulum formation and aggregation phenomena. Another kind of magnetic bead containing a polymeric core was produced by emulsion polymerisation of S in the presence of both PS seed and small iron oxide particles stabilised by a surfactant. The final magnetic polymer microspheres exhibited an uneven surface formed by small PS particles containing iron oxides [24].

Hydrophilic magnetic polymer particles were also obtained by Kondo et al. [27] using a two-step polymerisation method: emulsion polymerisation of S in the presence of iron oxide nanoparticles was followed by precipitation polymerisation of *N*-isopropylacrylamide (NIPAM) and methacrylic acid.

All these methods lead to magnetic particles exhibiting a wide range of size and encompassing various types of polymer. Nevertheless, none of these processes lead to the production of both monodisperse and hydrophilic submicron-sized magnetic particles.

The objective of this series of two papers is to present a new approach for the preparation of monosized hydrophilic magnetic latex particles for biomedical applications. The strategy developed here was derived from the work of Furuzawa et al. [29] and consisted of:

1. The initial preparation of anionic iron oxide nanoparticles and cationic latex particles.
2. Adsorption of negatively charged inorganic particles onto various seed polymer particles.
3. Encapsulation of adsorbed iron oxide nanoparticles onto seed latexes.

In this first paper, the adsorption of iron oxide nanoparticles is examined using three cationic seed latexes: PS, a core–shell P(S/NIPAM) and PNIPAM microgel particles. The influence of both charge and cross-link densities of the hydrogel shell layer on the adsorption process was investigated. Finally, the adsorption of iron oxide particles onto cross-linked PNIPAM particles was studied for comparison.

Experimental

Materials

Unless stated otherwise, reagents and solvents were used as received. Water was Milli-Q grade (Millipore, France) and was boiled for 2 h under α nitrogen stream before use. S (Janssen Chemica, France) was distilled under reduced pressure. NIPAM, from Kodak, was recrystallized in a 60/40 hexane/toluene mixture. 2,2′-Azobis(2-amidinopropane) dihydrochloride (V50), from Wako Chemical, was recrystallized from a 50/50 acetone/water mixture, and was used as the initiator for the seed cationic latex preparation. Aminoethyl methacrylate hydrochloride (AEM), from Kodak, *N*,*N*-methylene bisacrylamide (MBA), from Aldrich, $FeCl_2 \cdot 4H_2O$ (Merck), $FeCl_3 \cdot 6H_2O$ (Labosi), and trisodium citrate (Prolabo) were used as received. Bathophenanthroline disulfonic acid, disodium salt hydrate (Aldrich), and $FeSO_4 \cdot 7H_2O$ (Aldrich) were used for the chemical titration of iron oxide and *N*-succimidyl 3-(2-pyridyldithio) propionate (SPDP from Pierce) was used for the chemical titration of amidine and amine groups onto seed latex particles.

Synthesis of inorganic and polymeric colloids

Iron oxide dispersion

An iron oxide dispersion was prepared using the method already described [26, 31, 32, 33], based on the coprecipitation of $FeCl_2$ and $FeCl_3$ by adding a concentrated solution of base (10 M NaOH) onto the mixture of iron salts with a molar ratio ($FeCl_2/FeCl_3$) of 1/2. The alkaline solution was stirred for 1 h at 20 °C and was then heated at 90 °C for 1 h. The ultrafine magnetic particles obtained were peptized by a nitric acid solution (2 M). The iron oxide dispersion was then stirred for 30 min at 90 °C upon addition of a trisodium citrate solution (0.3 M). The excess citrate was removed by precipitation of ultrafine magnetic particles with acetone and by dialysis in water.

Cationic latexes

Three types of cationic latexes were prepared: cationic PS core–shell P(S/NIPAM) and hydrogel PNIPAM, all functionalized using AEM.

1. Cationic PS latexes (PS0, PS7, PS8, PS14) were prepared at 70 °C by soap-free batch emulsion copolymerization of S and AEM using V50 as the initiator. The synthesis and characterisation of such latexes was studied as a function of AEM concentration and is described elsewhere [34, 35].

2. Two series of cationic amino-containing NIPAM–S copolymer latexes were obtained by a shot-growth polymerisation process. The first series referred to as [P(S/NIPAM)3, P(S/NIPAM)10, P(S/NIPAM)12] was prepared at 70 °C at high conversion upon adding a mixture of NIPAM, MBA, V50 and AEM at various concentrations from 0 to 4 mol% over the NIPAM amount. The synthesis and characterisation were reported previously [36, 37]. The second series of core–shell particles [P(S/

NIPAM)24, P(S/NIPAM)25, P(S/NIPAM)26] were prepared in two steps: first a batch emulsion polymerisation step was carried out at 55 °C so as to obtain large particle sizes, and second shot addition of NIPAM, V50, AEM and MBA was performed at 70 °C at the end of the conversion by varying the MBA over the NIPAM amount from 1 to 6 mol%.

3. PNIPAM particles were synthesised by batch precipitation polymerisation at 70 °C of a NIPAM/MBA/AEM mixture and V50, and their characterisation as a function of cross-linking and functional monomer concentration was reported elsewhere [38]. Only one PNIPAM latex was used here to compare the adsorption of magnetic nanoparticles with the other series of latexes.

Adsorption of iron oxide nanoparticles onto latex particles

Adsorption of iron oxide particles was performed onto the various latex samples in order to obtain stable heterocoagulates. An iron oxide dispersion (0–5 g/l) and latex particles (2 g/l) were incubated at room temperature for 15 min in a 2-ml aliquot of a 5×10^{-3} M citrate solution at pH 6. The number of magnetic particles adsorbed onto the polymer microspheres (N_{ads}) was determined from the difference between the initial and the final iron oxide particle concentration by optical density measurements. The calibration of optical density (at a wavelength of 800 nm with an Uvikon 930 spectrophotometer) versus iron oxide particle concentration, ranging from 0 to 2 g/l, was used to quantify the free iron oxide particles.

Characterisation of iron oxide nanoparticles

Crystallographic structure of iron oxide

A crystallographic study was performed on an iron oxide powder by X-ray diffraction using Co Kα radiation (Centre de diffractométrie H. Longchambon, Université C. Bernard, Villeurbanne). The distances between peaks, d, were calculated according to Bragg's law and were compared to the ASTM X-ray diffraction data card so as to deduce the crystal structure.

Magnetic properties of the iron oxide dispersion

Magnetic measurements were carried out on the Automatic Bench of Magnetic Measurements CNRS-IRC, Villeurbanne. Magnetisation of the iron oxide dispersion was investigated by decreasing the magnetic field (H) from +20000 to −500 œrsted. The diamagnetic value of water was subtracted in order to take into account only the magnetic properties of the ultrafine particles.

Particle size determination

X-ray diffraction. The breadth of the peak obtained by X-ray diffraction depends on the apparatus and on the crystal size. For very small particle sizes (below 100 nm), broadening from the apparatus is negligible and Scherrer's formula [39] permits calculation of the crystal size:

$$D_{RX} = \frac{0.9 \times \lambda}{\Delta \cos \theta} \quad , \tag{1}$$

where 0.9 is a dimensionless constant of the equipment, λ, is the wavelength of the radiation corresponding to the Co K^{α}, peak and θ, is Bragg's angle.

Transmission electron microscopy. Transmission electron microscopy (TEM, Phillips CM120, CMEABG, C. Bernard University, Lyon I, France) permits the determination of the number-average diameter ($\overline{D_n}$) and the polydispersity index (PDI) of latex particles.

Magnetic measurements. Magnetic measurements allow evaluation of the particle size. Assuming the particles are superparamagnetic and that the volume fraction is below 1%, the magnetisation variation as a function of the applied magnetic field, H (G or 4 kA/m), can be described by Langevin's equation [40]:

$$M = M_s \left[\coth\left(\frac{\mu H}{kT}\right) - \frac{kT}{\mu H} \right] \quad , \tag{2}$$

where μ is the magnetic moment of each particle (A m^2), k is Boltzmann's constant, T is the absolute temperature and M_s is the saturation magnetisation (G or 4 kA/m).

For low and high magnetic fields, the reduced Langevin's equation can be used to calculate large (D_1) and small (D_2) magnetic particle diameters, respectively. Only particles of large size were oriented at low magnetic fields and D_1 was defined as

$$D_1 = \frac{18kT}{\rho_s \pi H} \left(\frac{dM}{dH}\right)_{H=0} \quad , \tag{3}$$

where ρ_s is the specific magnetisation of the iron oxides, with a value of 89.9 emu/g for (Fe_3O_4) [41]. On the other hand, the size of the small particles, D_2, was determined with a high magnetic field:

$$D_2 = \left(\frac{6kT}{\rho_s \pi H} \frac{M_s}{M_s - M(H)} \right)^{1/3} \quad . \tag{4}$$

Determination of the content of magnetic nanoparticles in aqueous media

The iron oxide contents were determined by both a physical and a chemical method.

1. Magnetic measurement allows determination of the saturation magnetisation (M_s) which corresponds to the saturation of the magnetisation at a high magnetic field value. The weight percentage of iron oxide ($\%W_{\text{iron oxide}}$) in aqueous solution was calculated using the experimental M_s value as follows:

$$\%W_{\text{iron oxide}} = 4300 \frac{M_s}{\rho_s W_{\text{sample}}} \quad , \tag{5}$$

where W_{sample} is the weight of the sample used for the measurements and 4300 is an apparatus constant.

2. The chemical titration was based on the complexation reaction of bathophenanthroline disulfonic acid disodium and Fe^{2+} ion in an acidic medium [26, 42]. The calibration curve was established using $FeSO_4$ solution concentrations ranging from 0 to 60 μg/l. In the acidic reaction medium, iron oxide particles were dissociated into Fe^{2+} ions. The optical density of the red complex was measured at 535 nm using a Uvikon 930 spectrophotometer. In addition, the adsorption of the iron oxide nanoparticles was qualitatively observed at the polymer particles' surface by scanning electron microscopy (Hitachi S800).

Characterisation of cationic polymer latexes

Particle size and distribution

The particle size and distribution of the polymer particles were determined by TEM providing $\overline{D_n}$ and PDI. In addition, quasi-elastic light scattering (QELS) (N4MD from Coultronics, France) was used to determine the hydrodynamic diameter D_h in a 10^{-3} M NaCl solution of latex particles at 20 and 40 °C.

Electrophoretic mobility measurements

Experiments were performed with a Zeta Sizer III (Malvern Instruments, England) at 20 and 40 °C.

Surface charge titration

The surface charge density of the seed latexes was determined using a chemical method based on the reaction of SPDP with the amino and amidino groups originating from initiator fragments and the AEM monomer, respectively. Details of the surface charge titration method are described elsewhere [35, 43].

Results and discussion

Colloidal properties of cationic seed latexes

Particle diameter, size distribution, surface charge density (σ) and electrophoretic mobility (μ_E) were determined at room temperature in the case of hydrophobic cationic PS particles instead of at 20 and 40 °C as for the hydrophilic cationic latexes.

Particle diameter and size distribution

The particle diameter and size distribution are reported in Table 1. TEM micrographs show that all latexes exhibit a PDI close to 1.05, reflecting the narrow size dispersity of the seed latexes. Upon increasing the AEM concentration, the PS particle size (D_h, $\overline{D_n}$) decreases. Such a trend was generally observed in soap-free batch emulsion copolymerization of S with a functional monomer [44]. The presence of the ionic functional monomer enhances particle stability during the nucleation period, and so more particles are formed and the final latex particles have a small size [34, 35].

The hydrodynamic diameter of the hydrophilic particles, measured at 40 °C using QELS, is lower than that measured at 20 °C. The shrinkage of the particles is due to the thermal sensitivity of NIPAM which exhibits a lower critical solubility temperature (LCST) near 32 °C. At room temperature, NIPAM is in a swollen state due to hydrogen bonding between water and amide groups, whereas above 32 °C water is released out of the particles. In addition, the measured diameters of core–shell latexes in the dried state (from TEM) are smaller than those obtained above the LCST.

Electrophoretic measurements

The electrophoretic mobility (μ_E) of the cationic seed latex was investigated as a function of pH at 20 °C and 10^{-3} M NaCl. The results shown in Fig. 1 show that μ_E is positive in a pH range from 3 to 9. Upon increasing the pH, cationic groups are progressively neutralised leading to a decrease in the absolute surface charge density. The negative μ_E value above the isoelectric point (IEP) of both latexes was attributed to carboxylic groups originating from the hydrolysis of amidino groups as reported by Goodwin et al. [45].

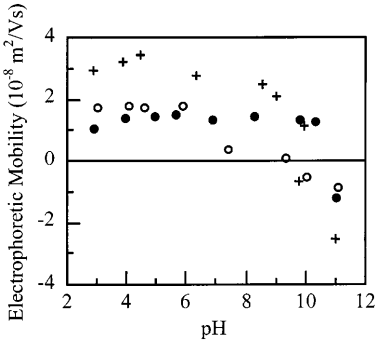

Fig. 1 Electrophoretic mobility of cationic latexes as a function of pH at 20 °C, 10^{-3} M NaCl. Polystyrene (*PS*) PS14 (+); core–shell latexes P(S/N-isopropylacrylamide (*NIPAM*)) (●); P(S/NIPAM)24 (○)

Table 1 Hydrodynamic diameter (D_h) and number average diameter ($\overline{D_n}$), polydispersity index (*PDI*), hydrophilic layer thickness (δ) and surface charge density (σ) of the cationic latexes made from polystyrene (*PS*) and *N*-isopropylacrylamide (*NIPAM*), with *N*,*N*-methylene bisacrylamide (*MBA*) and aminoethyl methacrylate hydrochloride (*AEM*)

Latex	%MBA[a]	%AEM[b]	D_h (20 °C) (nm)	D_h (40 °C) (nm)	$\overline{D_n}$ (nm)	PDI	δ[c] (nm)	σ (μmol/g)
PS0	0	0	620	–	473	1.001	–	23
PS14	0	0.15	360	–	320	1.002	–	22
PS8	0	0.35	205	–	185	1.002	–	31
PS7	0	0.7	150	–	145	1.016	–	33
P(S/NIPAM)10	1	0	600	365	288	1.010	117	7
P(S/NIPAM)3	1	2	570	325	320	1.050	122	21
P(S/NIPAM)12	1	3	485	335	300	1.004	75	35
P(S/NIPAM)24	1	2	695	550	475	1.010	72	11.5
P(S/NIPAM)25	3	2	690	540	473	1.020	75	10.5
P(S/NIPAM)26	6.15	2	730	555	543	1.020	87	10
PNIPAM92	6.2	0.5	450	215	149	ND	117	10.7

[a] MBA molar percentage over amount of NIPAM
[b] AEM molar percentage over amount of NIPAM
[c] δ defined as $(D_{h(20°C)} - D_{h(40°C)})/2$
ND Not determined

The difference in the IEP between samples PS14, P(S/NIPAM)3 and (PNIPAM92) can be attributed to the presence of the hairy layer and to the charge distribution in the hydrogel layer. The presence of such a layer causes a shift of the slipping plane, inducing a change in the electrokinetic behaviour as a function of pH, as already observed by several authors [37, 46].

Properties of ultrafine magnetic particles

Many different natural structures of iron oxide exist such as magnetite (Fe_3O_4), hematite (α-Fe_2O_3), maghemite (γ-Fe_2O_3), martite (Fe_2O_3) or ferric hydroxide (β-FeOOH) [50]. They all exhibit magnetic properties. The nature of iron oxide was first determined by X-ray diffraction, then particle size and magnetic properties were studied.

Crystallographic structure

X-ray diffraction patterns lead to the determination of the crystallographic structure of iron and iron oxide types. Experimental d spacings obtained from X-ray diffraction patterns are reported in Table 2 and are similar to the ASTM data cards of both the Fe_3O_4 and γ-Fe_2O_3 structures, which exhibit the same inverse spinel structure [47, 48]. Based on the d spacing and on the preparation method, it can be concluded that a mixture of both iron oxides was obtained.

Particle size of iron oxide dispersion

The results are listed and compared in Table 3. All methods give a diameter between 5 and 10 nm which is a common value for superparamagnetic iron oxide as reported by different authors [49–51]. In contrast, larger-sized particles obtained using atomic force microscopy can be attributed to the sensitivity of this technique, since tip artefacts may distort and enlarge the shape of small spherical particles.

Table 2 Experimental d (Å) spacings from X-ray patterns, [d (exp)], and d spacings from ASTM data cards for two types of iron oxide [d (Fe_3O_4), d (γFe_2O_3)]

d (exp)	d (Fe_3O_4)	d (γFe_2O_3)
4.79	4.852	4.82
3.01	2.967	2.95
2.52	2.532	2.52
2.09	2.0993	2.08
1.61	1.6158	1.61
1.48	1.4845	1.48

Table 3 Iron oxide particle size according to different characterisation methods

Particle diameter (nm)		Method
$\overline{D_n} = 13$	$\overline{D_w} = 18$	Atomic force microscopy
$\overline{D_n} = 7$	$\overline{D_w} = 8.5$	Transmission electron microscopy
$D_2 = 5.5$	$D_1 = 9$	Magnetisation
10		X-ray

Magnetic properties

The magnetisation variation (M) versus the applied magnetic field (H) (Fig. 2) provides information on the magnetic properties of the iron oxide. Upon decreasing the magnetic field, the magnetisation of iron oxide particles decreases from the plateau value and reaches zero at $H = 0$. At a low negative magnetic field, no residual magnetisation and remanence are observed. Since the particle size of iron oxide is about 10 nm, each particle corresponds to a single crystal domain exhibiting only one orientation of the magnetic moment. This explains why no remanence is observed and the iron oxide exhibits superparamagnetic properties [48, 52].

In addition, the saturation magnetisation (M_s) is found to increase when the volume fraction (Φ) of ultrafine particles increases. This can be attributed to the relationship between M_s, the saturation magnetisation of a single particle (m_s) and the volume fraction ($M_s = \Phi m_s$) [40], which explains the observed behaviour depicted in Fig. 2.

Surface charge density

The surface charge density of iron oxide particles could not be evaluated due to experimental problems to perform titrations with such tiny inorganic particles. The nanoparticles obtained are therefore assumed to be negatively charged according to the preparation method reported by Bacri et al. [53]. Indeed, the iron oxide nanoparticles prepared by these authors were negatively charged, with a -0.2 C/m^2 surface charge density as determined by conductometric titration [31].

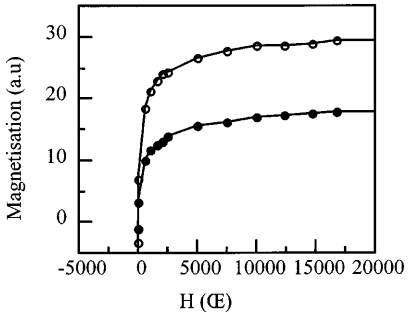

Fig. 2 Magnetisation curve of ultrafine particles at different volume fractions. Φ = 0.34 (○); Φ = 0.21 (●)

Adsorption of iron oxide nanoparticles onto cationic latexes

The adsorption medium was chosen to be similar to that of the iron oxide dispersion: 3×10^{-2} ionic strength and pH = 6 were kept constant in all samples. At this pH, the latex particles are positively charged and the ultrafine magnetic particles negatively charged [53] as shown in Fig. 3. Adsorption was performed on the three polymer colloid models differing in their interfacial properties.

Adsorption onto PS particles

The adsorption isotherm onto the PS latex represents the amount of iron oxide adsorbed (N_{ads}) in grams per gram of polymer particles as a function of the equilibrium concentration of nanoparticles as illustrated in Fig. 4. Two domains are clearly evidenced:

1. A rapid increase in the interfacial concentration (N_{ads}) of the low nanoparticle concentrations reflects the high affinity between both types of particles.
2. A plateau value is reached for high amounts of iron oxide dispersion.

The same trend was observed for adsorption isotherms obtained from all the cationic latexes, except that the maximum adsorbed at the plateau value strongly depends on the nature of the latex surface.

The results obtained from the adsorption study carried out on PS particles exhibiting various charge densities are reported in Table 4. With decreasing particle diameter, the amount of iron oxide adsorbed per gram of polymer microspheres is found to increase since small particles provide a large specific surface area. In contrast, the maximum amount of iron oxide nanoparticles adsorbed is found to be constant (0.8–0.9 $\mu g\ cm^{-2}$) irrespective of the surface charge density (Table 4). In all cases, the overall surface area of the polymer particles is coated by iron oxide nanoparticles and even if more cationic charges are available no more small particles can be added, indicating that the adsorption saturation point is reached.

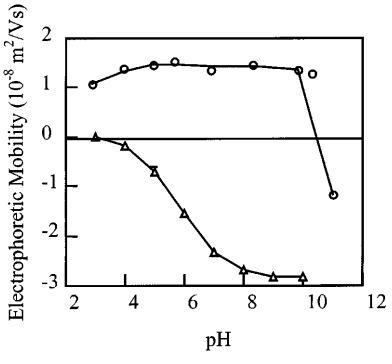

Fig. 3 Electrophoretic mobility of different types of particles as a function of pH at 20 °C. (Bare latex P(S/NIPAM)3 (○); iron oxide (▲) from Ref. [54]

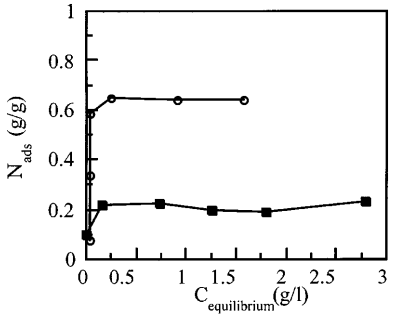

Fig. 4 Adsorption isotherms of iron oxide onto PS and core–shell particles at room temperature, pH 6 and 3×10^{-2} ionic strength. PS14 (■) ; P(S/NIPAM)3 (○)

Table 4 Amount of iron oxide adsorbed (N_{ads}) onto various PS particles

Run	σ (μmol/g)	N_{ads} (g/g)	N_{ads} (μg/cm^2)
PS0	23	0.10	0.82
PS14	22	0.16	0.89
PS8	31	0.27	0.87
PS7	33	0.35	0.88

Since iron oxide particle adsorption is principally governed by electrostatic interactions, the amount adsorbed onto such smooth particles is limited by lateral repulsive interactions irrespective of the surface charge density. In addition, the adsorption of iron oxide nanoparticles onto PS particles was viewed by observation of TEM micrographs (Fig. 5) of the initial seed and the coated particles. Then, the adsorption of iron oxide particles onto cationic core–shell P(S/NIPAM), i.e. bearing a charged hairy layer, in order to increase the amount of iron oxide adsorbed was examined.

Adsorption onto P(S/NIPAM) particles

The maximum number of ultrafine particles adsorbed onto P(S/NIPAM) latexes was found to be larger than that reported for the cationic PS latex (Fig. 4). Both latexes have the same charge density and particle diameter. Such an increase can be attributed to the presence of the charged hairy layer in these core–shell latexes. In this case, cationic groups are randomly distributed within the volume of the hydrophilic layer and they are more accessible to the small inorganic particles. On the other hand, in the case of PS particles, cationic charges are only located at the particle surface, therefore maximum surface coverage is reached at lower iron oxide particle concentrations and as already suggested lateral electrostatic repulsions induce a limitation in the number of iron oxide nanoparticles adsorbed.

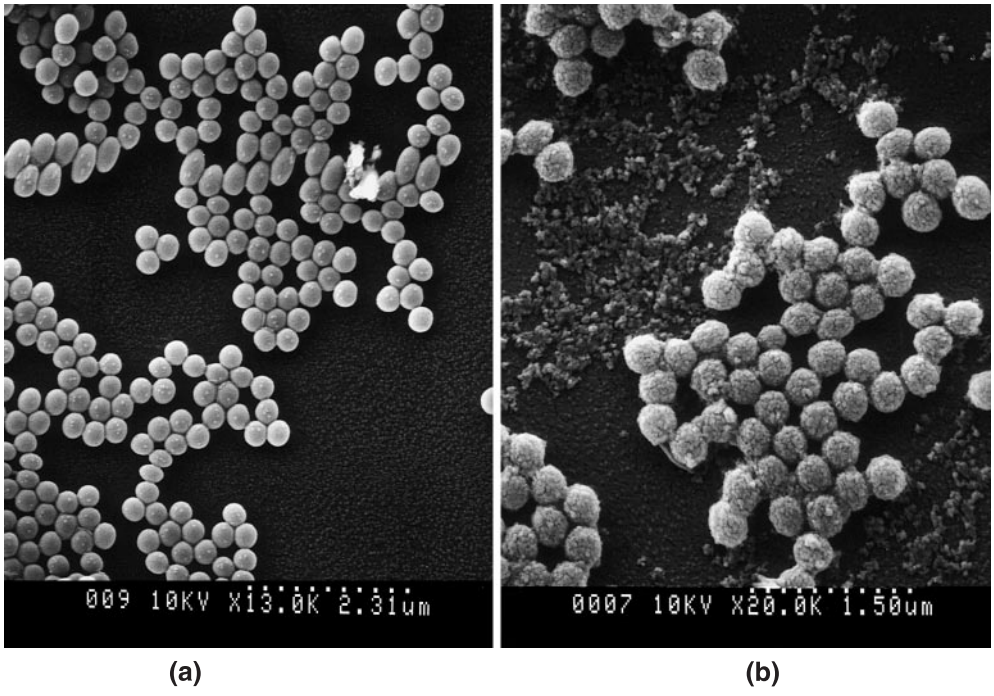

Fig. 5a,b Scanning electron microscope micrographs. **a** PS14 (×10000); **b** PS14 coated with iron oxide particles (×22000)

In addition to electrostatic interactions between both oppositely charged particles, diffusion of iron oxide nanoparticles inside the hydrophilic shell acts to increase the number of small particles adsorbed. This can be explained by both magnetic and polymer particle properties. At room temperature, the PNIPAM shell can contain up to 90% of water. When the hydrophilic latex is mixed with the iron oxide particles, the magnetic nanoparticles tend to penetrate inside the charged hairy polymer particles until an equilibrium is reached in spite of steric hindrance. Moreover, the cationic charges on the P(S/NIPAM) particles are located within the hairy layer and can create long distant coulombic interactions causing the nanoparticles inside the hydrophilic layer.

Assuming that adsorption was driven both by electrostatic interactions and diffusion into the PNIPAM layer, adsorption isotherms were determined using core–shell particles with hydrophilic shells having different charges and cross-linking densities. The particle surface is not well defined below the LCST in the presence of the hairy layer. Nevertheless, since P(S/NIPAM) of each series have almost identical diameters, the amounts adsorbed are first discussed in terms of weight of iron oxide per weight of polymer particles and not in terms of weight of iron oxide particles per surface unit.

Figure 6 shows that the three adsorption isotherms exhibit the same trend with the amount of iron oxide adsorbed increasing with the polymer particle charge density. Since more cationic groups are available in the hydrophilic surface layer, more small particles are adsorbed through electrostatic interactions. It is worth noting that an increase in AEM concentration in the shot-growth polymerisation recipe affects both surface charge density and hydrophilic layer thickness of the core–shell particles. Although the PNIPAM shell thickness decreases, the increase in surface charge density, as a consequence of electrostatic interactions, allows a greater amount to be adsorbed. Nevertheless, according to the increase in the plateau adsorption values reported in Table 5, the hydrophilic layer is probably not yet saturated by iron oxide nanoparticles. Using a latex exhibiting a higher charge density could have further increased the adsorption plateau.

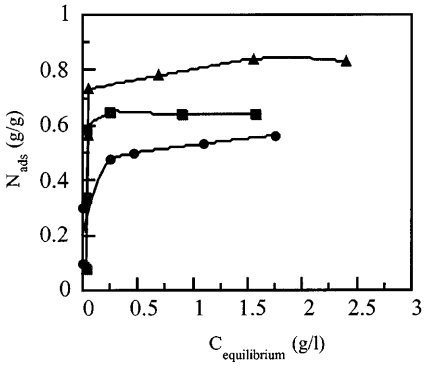

Fig. 6 Adsorption isotherms of iron oxide onto core–shell latexes at room temperature, pH 6 and 3×10^{-2} ionic strength as a function of surface charge density. 0% aminoethyl methacrylate hydrochloride (*AEM*) (▲); 2% AEM (■); 3% AEM (●)

In contrast, when increasing the amount of MBA in order to cross-link the hydrophilic shell around the iron

Table 5 Maximum amount of iron oxide adsorbed, N_{ads} (g/g) and experimental coverage ratios (θ_h), and (θ_n) calculated using the hydrodynamic diameter at 20 °C (D_h) and the number-average diameter (D_n) respectively

Latex	σ (μmol/g)	$D_{h\,20°C}$ (nm)	N_{ads} (g/g)	(θ_h)	(θ_n)
PS0	23	620	0.10	0.55	0.42
PS14	22	360	0.16	0.50	0.44
PS8	31	205	0.27	0.46	0.41
PS7	33	150	0.35	0.42	0.41
P(S/NIPAM)10	7	600	0.55	2.94	1.36
P(S/NIPAM)3	21	570	0.64	3.25	1.77
P(S/NIPAM)12	35	485	0.83	3.55	2.25
P(S/NIPAM)24	11.5	695	0.37	2.3	1.55
P(S/NIPAM)25	10.5	690	0.30	1.85	1.26
P(S/NIPAM)26	10	730	0.25	1.64	1.10
PNIPAM92	10.5	450	1.24	4.96	1.51

oxide particles, the plateau value decreases (Fig. 7). In this case, incorporation of nanoparticles into the hydrogel layer is reduced due to the increase of the cross-linking density in the hairy layer. Nevertheless, the MBA concentration cannot be lowered in the recipe to below 1 mol% over the NIPAM amount in order to prevent the formation of too high a yield of water-soluble polymer released when the temperature is lowered below the LCST. Comparing two differently sized core–shell latexes obtained according to the same recipe, the amount of iron oxide adsorbed onto P(S/NIPAM)24 is lower than that adsorbed onto P(S/NIPAM)3. As shown in Table 1, for P(S/NIPAM)3 the hairy layer is thicker than that of P(S/NIPAM)24 and iron oxide can diffuse more easily.

It can be concluded that adsorption of iron oxide nanoparticles can be increased by using polymer particles exhibiting a large hydrogel layer, with a low cross-linking density and high charge density.

Adsorption onto P(NIPAM) latex particles

When using hydrogel PNIPAM particles (sample PNIPAM92), the amount of iron oxide adsorbed increases greatly (Table 6). In the presence of the large water-swollen hydrogel structure, diffusion of iron oxide nanoparticles can take place within a large part of the whole particle. Adsorption is found to increase in comparison with the amount obtained using core–shell particles. In spite of a relatively low charge density (10.7 μmol/g) and a high MBA amount (6%), the number of iron oxide nanoparticles adsorbed is still important.

Since temperature has a dramatic effect on core–shell and PNIPAM particle size, adsorption was also carried out at 40 °C. The results reported in Table 6 show a significant decrease in N_{ads} above the LCST. Particle diameters and, as a consequence, available diffusion volumes, decrease above 32 °C. Moreover, the difference between 20 and 40 °C is more important in the case of PNIPAM latex samples than core–shell particles because the hydrodynamic volume is reduced by 14% from the volume at 20 °C (Table 6). Even at 40 °C, the amount of iron oxide adsorbed is higher with PNIPAM92 than with the core–shell P(S/NIPAM) particles.

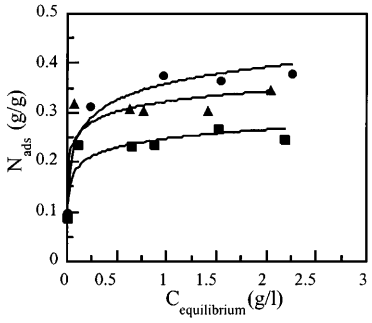

Fig. 7 Adsorption isotherms of iron oxide onto core–shell latexes at room temperature, pH 6 and 3×10^{-2} ionic strength as a function of cross-linking density. 1% *N,N*-methylene bisacrylamide (*MBA*) (●); 3% MBA (■); 6% MBA (▲)

Table 6 Hydrophilic particle hydrodynamic diameter (D_h) and maximum amount of iron oxide adsorbed (N_{ads}) at 20 and 40 °C

Seed latexes	D_h (nm)		N_{ads} (g/g)	
	20 °C	40 °C	20 °C	40 °C
PNIPAM92	450	215	1.24	0.95
P(S/NIPAM)24	695	550	0.37	0.3

Discussion and conclusions

A study of the adsorption of anionic iron oxide nanoparticles onto various cationic latex particles was performed. Electrophoretic mobility measurements allowed the cationic and anionic character of the seed latexes and the character of iron oxide nanoparticles to be revealed. On the whole, the adsorption behaviour of iron oxide nanoparticles onto polymer particles was performed under conditions (pH domain) favouring the electrostatic attractive forces between the two colloids (iron oxide nanoparticles and latex particles).

Firstly, the adsorption of iron oxide nanoparticles onto smooth PS latex particles was investigated. The

maximum number of iron oxide nanoparticles adsorbed was found to be independent of the surface charge density within the domain investigated. The behaviour observed reflected the fact that the minimum surface charge density found in this work is high, as pointed out by the effect of surface charge density on the maximum amount of iron oxide adsorbed. In fact, the surface coverages (θ_n) reported in Table 5 are lower than 54%, corresponding to the maximum surface coverage calculated from the random sequential adsorption simulation. Furthermore, the surface coverages obtained reflect the formation of a monolayer.

Secondly, the adsorption of iron oxide particles onto core–shell PS-PNIPAM latexes was studied as a function of charge concentration and cross-linking density of the hydrophilic shell. One important result is that the adsorption of iron oxide nanoparticles increases when the seed latexes bear a hydrophilic shell. This difference in adsorption behaviour can be attributed to the diffusion of nanoparticles inside the charged hydrogel layer leading to adsorption in the shell volume instead of on the surface only as in the case of smooth particles. Moreover, surface coverages determined from the number of iron oxide nanoparticles adsorbed on the core–shell latexes using the hydrodynamic size at 20 °C have high values ($\theta_n > 0.54\%$) reflecting multilayer adsorption. Further, the maximum number of iron oxide nanoparticles adsorbed can be further increased by increasing the charge density (i.e. an increase in the attractive electrostatic interactions). In addition, the adsorption of small inorganic particles onto thermosensitive latexes was found to be not only affected by charge density but also by the cross-linking density of the polyelectrolyte layer: too high a cross-linking density reduced the diffusion of nanoparticles in the hydrogel polymer.

Finally, the adsorption of iron oxide onto pure cationic PNIPAM latexes was greater compared to the two other latexes. This behaviour can be due to the combined effect of the charge distribution and the cross-linker densities of the hydrogel particles on the attractive electrostatic interactions and the diffusion process of small oppositely charged nanoparticles onto the slightly cross-linked PNIPAM particles.

To ensure cohesion of the heterocoagulates of polymer latexes coated with iron oxide, encapsulation has been envisioned by polymerisation on both hydrophobic and hydrophilic particles. This will be presented in the second paper, taking into account the monomer mixture used in the polymerisation process as well as experimental conditions.

Acknowledgements The authors gratefully acknowledge the collaboration of G.A. Martin and P. Moral (IRC/CNRS, Villeurbanne) for the magnetic measurements, and A. Thozet and R.Vera (Centre de Diffractométrie, H.Longchambon, Lyon) for their help with X-ray diffraction measurements. The authors are also indebted to D. Duracher for the preparation of a few core–shell latexes.

References

1. Hofman-Caris CHM (1994) New J Chem. 18:1087
2. Haukanes B-I, Kvam C (1993) Biotechnology 11:60
3. Ugelstad J, Berge A, Ellingsen T, Schmid R, Nilsen T-N, Mork PC, Stenstad P, Hornes E, Olsvik O (1992) Prog Polym Sci 17:87
4. Setchell CH (1985) J Chem Technol Biotechnol 35B:175
5. Plastoucas CD (1987) In: El-Aasser MS, Fitch RM (eds) Future directions in polymer colloids. Nijhoff, Dordrecht, pp 321–355
6. Langer R (1990) Science 249:1527
7. Safarik I, Safarikova M, Forsythe S (1995) J Appl Bacteriol 78:575
8. Ugelstad J, Olsvik O, Schmid R, Berge A, Funderud S, Nustad K (1993) In: Ngo T (eds) Molecular interactions in bioseparation. Plenum, New York, pp 229–244
9. Lea T, Vartdal F, Nustad K, Funderud S, Berge A, Ellingsen T, Schmid R, Stenstad P, Ugelstad J (1988) J Mol Recognit 1:9
10. Widder KJ, Senyei AE, Scarpelli DG (1978) Proc Soc Exp Biol Med 58:141
11. Decun S, Jiaxiu S, Sha L, Qingshu L, Youfeng H, Yuxiao W, Huijuan C (1996) J Radioanal Nucl Chem 206:189
12. Nakamae K, Tanigawa S, Tsujiguchi T, Okamoto S, Yamaguchi K (1993) Colloids Surf A 80:85
13. Shimomura M, Kikuchi H, Yamaguchi T, Miyauchi S (1996) Pure Appl Chem A 33:1687
14. Müller-Schulte D, Füss F, De Cuyper M (1997) In: Häfeli U, Schütt W, Teller J, Zborowski M (eds) Scientific and clinical applications of magnetic carriers. Plenum, New York, pp 93–107
15. Hertzog B, Mottl T, Yim D, Mathiowitz E (1997) In: Häfeli U, Schütt W, Teller J, Zborowski M (eds) Scientific and clinical applications of magnetic carriers. Plenum, New York, pp 77–92
16. Widder K, Flouret G, Senyei A (1979) J Pharm Sci 68:79
17. Senyei A, Widder K, Czerlinski G (1978) J Appl Phys 49:3578
18. Ugelstad J, Stenstad P, Kilaas L, Prestvik WS, Herje R, Berge A, Hornes E (1993) Blood Purif 11:349
19. Olsvik O, Popovic T, Skjerve E, Cudjoe KS, Hornes E, Ugelstad J, Uhlen M (1994) Clin Microbiol Rev:43
20. Ugelstad J, Ellingsen T, Berge A, Helgee B (1986) European patent 0 106 873
21. Ugelstad J, Mork PC, Schmid R, Ellingsen T, Berge A (1993) Polym Int 30:157
22. Kawaguchi H, Fujimoto K, Nakazawa Y, Sakagawa M, Ariyoshi Y, Shidara M, Okazaki H, Ebisawa Y (1996) Colloids Surf A 109:147
23. Charmot D (1989) Prog Colloid Polym Sci 76:94
24. Lee J, Senna M (1995) Colloid Polym Sci 273:76
25. Huang T-CC (1986) Thesis. Lehigh University, Bethlehem, USA
26. Tourinho FA, Franck R, Massart R (1990) J Mater Sci 25:3249
27. Kondo A, Kamura H, Higashitani K (1994) Appl Microbiol Biotechnol 41:99
28. Yanase N, Noguchi H, Asakura H, Suzuta T (1993) J Appl Polym Sci 50:765
29. Furusawa K, Nagashima K, Anzai C (1994) Colloid Polym Sci 272:1104

30. Bourgeat-Lami E, Espiard P, Guyot A (1995) Polymer 36:4385
31. Jolivet JP, Massart R, Fruchart J-M (1983) Nouv J Chim 7:325
32. Tourinho FA, Franck R, Massart R, Perzynski R (1989) Prog Colloid Polym Sci 79:128
33. Neveu-Prin S (1992) Thesis. P. et M. Curie University, Paris, France
34. Ganachaud F, Sauzedde F, Elaïssari A, Pichot C (1997) J Appl Polym Sci 65:2315
35. Sauzedde F, Ganachaud F, Elaïssari A, Pichot C (1997) J Appl Polym Sci 65:2331
36. Duracher D, Sauzedde F, Elaïssari A, Perrin A, Pichot C (1998) Colloid Polym Sci 276:219
37. Duracher D, Sauzedde F, Elaïssari A, Pichot C, Nabzar L (1998) Colloid Polym Sci 276:920
38. Meunier F, Elaïssari A, Pichot C (1995) Polym Adv Technol 6:489
39. Massart R, Cabuil V (1987) J Chim Phys 84:967
40. Bacri JC, Perzynski R, Salin D, Cabuil V, Massart R (1986) J Magn Magn Mater 62:36
41. Chikazumi S (1964) Physics of magnetism, Wiley J (ed). Krieger, p 100
42. Charlot G (1966) In: Les méthodes de la chimie analytique, Masson (ed), p 737
43. Delair T, Marguet V, Pichot C, Mandrand B (1994) Colloid Polym Sci 272:962
44. Van Streun KH, Belt WJ, Piet P, German AL (1991) Eur Polym J 27:931
45. Goodwin JW, Ottewill RH, Pelton R (1979) Colloid Polym Sci 257:61
46. Tamai H, Mukurami T, Suzawa T (1985) J Appl Polym Sci 30:3857
47. Losche M, Sackmann E, Mohwald H (1983) Ber Bunsenges Phys Chem 87:848
48. Smith J, Wijn HPJ (1968) Les ferrites Propriété des oxydes férimagnétiques en relation avec leur applications techniques. Dunod (ed)
49. Massart R, Dubois E, Cabuil V, Hasmonay E (1995) J Magn Magn Mater 149:1
50. Upadhyay RV, Davies KJ, Wells S, Charles SW (1995) J Magn Magn Mater 139:249
51. Shinkai M, Honda H, Kobayashi T (1991) Biocatal 5:61
52. Herpin A (1968) In: Théorie du magnétisme. Press Universitaire de France (PUF)
53. Bacri JC, Perzynski R, Salin D, Cabuil V, Massart R (1990) J Magn Magn Mater 85:27
54. Bacri JC, Perzynski R, Salin D, Cabuil V, Massart R (1989) J of Colloid interface Sci, 1, 132